Automatic Classification of General Movements in Newborns

Daphné Chopard^{1,2*}
Sonia Laguna^{1*}
Kieran Chin-Cheong^{1*}
Annika Dietz³
Anna Badura³
Sven Wellmann³
Julia E Vogt¹

DAPHNE.CHOPARD@INF.ETHZ.CH
SONIA.LAGUNACILLERO@INF.ETHZ.CH
KIERAN.CHINCHEONG@INF.ETHZ.CH
ANNIKA.DIETZ@STUD.UNI-REGENSBURG.DE
ANNA.BADURA@BARMHERZIGE-REGENSBURG.DE
SVEN.WELLMANN@BARMHERZIGE-REGENSBURG.DE
JULIA.VOGT@INF.ETHZ.CH

¹Department of Computer Science, ETH Zurich, Switzerland; ²Department of Intensive Care and Neonatology and Children's Research Center, University Children's Hospital Zurich, University of Zurich, Switzerland; ³Department of Neonatology, Children's University Hospital Regensburg (KUNO), Hospital St. Hedwig of the Order of St. John, University of Regensburg, Regensburg, Germany

Abstract

General movements (GMs) are spontaneous, coordinated body movements in infants that offer valuable insights into the developing nervous system. Assessed through the Prechtl GM Assessment (GMA), GMs are reliable predictors for neurodevelopmental disorders. However, GMA requires specifically trained clinicians, who are limited in number. To scale up newborn screening, there is a need for an algorithm that can automatically classify GMs from infant video recordings. This data poses challenges, including variability in recording length, device type, and setting, with each video coarsely annotated for overall movement quality. In this work, we introduce a tool for extracting features from these recordings and explore various machine learning techniques for automated GM classification.

Keywords: Automated General Movements Assessment (GMA), Neurodevelopmental Disorder Screening Tool, Time Series, Paediatrics

Data and Code Availability The private dataset consists of infant videos collected by the Barmherzige Brüder Regensburg Hospital, details in Section 2.1 and Appendix A. The code¹ is publicly available.

Institutional Review Board (IRB) IRB project 23-3304-104: "Development of a Computer tool for the Assessment of General Movements".

1. Introduction and Related Work

General movements (GMs) refer to spontaneous movements of the entire body observable in infants from early fetal life until approximately six months post-term (Einspieler and Prechtl, 2005). These movements include coordinates sequences of the arms, legs, neck, and trunk, with variations in intensity, force, and speed. GMs are inherently complex, variable, and fluid, and their quality can provide critical insights into the integrity of the developing nervous system. Assessing GM quality, known as the Prechtl General Mouvement Assessment (GMA), is a sensitive and reliable diagnostic tool for predicting the likelihood of cerebral palsy and other neurodevelopmental disorders (Einspieler and Prechtl, 2005). The types of movements predictive of later neurodevelopmental disorders vary significantly with age, and age-based distinctions are essential when studying newborns. From early fetal life until approximately two months post-term, GMs exhibit consistent writhing movements. Between 6 to 9 weeks post-term, these writhing patterns diminish, and fidgety movements emerge, persisting until around the middle of the first year of life, at which point intentional movements become predominant. Alterations in these movement patterns can indicate later disorders. While GMA is typically conducted in hospitals by specialized clinicians, there are too few trained experts to screen all newborns. This motivates the need to develop a tool for automatic and reliable classification of movements.

Initial attempts at addressing this challenge focused on computer-based approaches using feature

^{*} These authors contributed equally

^{1.} https://github.com/chopardda/GMA

extraction techniques (Baccinelli et al., 2020; Raghuram et al., 2022). However, recent advances in deep learning and computer vision have spurred the development of more sophisticated methods (Silva et al., 2021; Irshad et al., 2020). For instance, Reich et al. (2021) proposed to use a pose estimator, OpenPose, to extract skeletons and used these as input to a shallow multilayer neural network to discriminate between movements. Other deep learning solutions, e.g. by Schmidt et al. (2019), work in controlled conditions. Despite their promise, these approaches often rely on controlled environments with fixed sensors and constant recording length, limiting their scalability and applicability in real-world clinical settings.

In this work, we present a preliminary study introducing a method to label key anatomical points, automatically process videos, and classify GMs based on the tracked anatomical points across videos, using a dataset from Barmherzige Brüder Regensburg Hospital. The challenges posed by the variability in recording lengths and devices, the diversity of video scenarios (including both hospital and home environments), and the nature of the movement quality annotations—one per recording—are significant for reliable GM classification. Addressing these challenges is crucial to the generalization of an automatic GMA that can be effectively deployed in varied settings. The goal is to enable comprehensive newborn screening and follow-up studies by experts, ultimately improving the early detection and treatment of neurodevelopmental disorders.

2. Dataset and Methods

This work involves labelling specific anatomical landmarks of interest—so-called *keypoints* (*KP*)—in video frames (Section 2.2), tracking their positions across the video (Section 2.2), and extracting features from the tracked keypoints (Section 2.4) to classify movement quality. The full pipeline is illustrated in Figure 1.

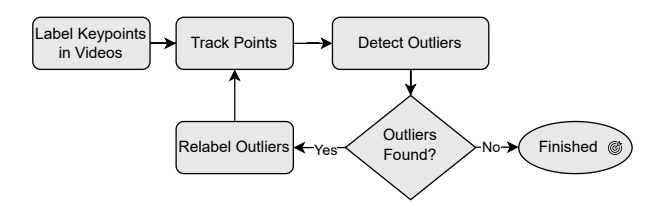


Figure 1: Flowchart of keypoint extraction pipeline after initial video resampling and cropping.

2.1. Dataset

This study includes 76 infant video recordings collected from the Barmherzige Brüder Regensburg Hospital. The dataset is highly heterogeneous, including videos recorded both at home and in hospital settings using various recording devices, resulting in differing resolutions and frame rates. There is also significant variability in camera angles and orientations, distance from subject to camera, infants' clothing, and background types, among other factors.

The data is split into two age-based groups: the early infancy group includes 39 infants with a postmenstrual age of up to 37 weeks, while the late infancy group consists of 37 infants with postmenstrual ages ranging from 46 to 56 weeks. Each sample is associated with a binary label that classifies the infant's movement quality. In the early group, labels distinguish between normal and poor movement repertoire, while in the *late* group, labels indicate normal or absence of fidgety movements, following Einspieler and Prechtl (2005). To minimize bias and improve reliability, two trained physicians independently annotated the videos. In cases of disagreement, the recordings were reviewed jointly until a consensus label was reached. In the dataset, 24 infants in the early group exhibit poor repertoire, while 10 in the late group lack fidgety movements.

2.2. Keypoint Retrieval Tools

Keypoint Labelling We introduce a keypoint labelling tool based on the work from Doersch et al. (2022) to mark sets of key coordinates in the videos, which, along with point tracking, forms the backbone of the preprocessing pipeline. The tool allows labelling of extremities such as wrists and ankles—referred to as extreme keypoints, as well as additional joints such as elbows, hips, and knees—collectively referred to as all keypoints, totaling 17. In this study, three independent non-expert labellers manually labelled all keypoints for subsequent tracking. Full lists of relevant keypoints can be found in Appendix B, see Figure 2 a) for an illustration of the tool.

Point Tracking For tracking labelled keypoints across video frames, we utilize the point tracking algorithm proposed by Doersch et al. (2022). This approach predicts the trajectory of each point by extracting dense feature representations for every frame, leveraging a cost-volume approach. The cost volume measures the similarity between the feature of the tracked point in one frame and the features at

all possible locations in subsequent frames, encoding the probability of the tracked point's next position. A neural network then processes this cost volume to predict the tracked point's location across frames. More details are provided in Appendix C.



Figure 2: a) The point labelling tool prompts the user to label either only extreme keypoints or all keypoints. b) The outlier detection tool displays potential unrealistic point movements and allows manual correction.

2.3. Data Preprocessing

Due to the heterogeneity of the data, a robust preprocessing and error correction pipeline is necessary to prepare the videos for machine learning model development. This subsection outlines the key steps in that process, with a graphical overview in Figure 1.

Resampling and Extreme Keypoints Labelling Preprocessing begins with homogenizing all the video data by resampling to 30 frames per second. Extreme keypoints are then labelled. If all required keypoints are not visible in the first frame, labelling occurs in subsequent frames where visibility is clearer.

Video Cropping Next, the extracted extreme keypoints are tracked and used to apply a rectangular crop per video. The crop is determined by the most extreme values of the tracked points in each video, with a 15% margin to ensure the infant consistently occupies a similar portion of the video frame. This normalization step is crucial for maintaining consistency in the input data for machine learning models.

Outlier Detection To address inaccuracies in the tracking algorithm, such as when points jump inappropriately due to occlusions or overlapping limbs, an outlier detection mechanism is applied. The tool automatically flags any sudden and unrealistic movement of keypoints and prompts manual relabelling by the annotators, as shown in Figure 2 b). After relabelling, the affected keypoints are retracked. This process is iterated a fixed number of rounds, two in these results, or until no further outliers are detected, ensuring the accuracy of the tracked coordinates.

Final Data Preparation Prior to classification, the time series data must be homogenized. All video samples are split into fixed-length fragments corresponding to the shortest present recording, and zero-filling is applied to any occluded or missing coordinates. To prevent data leakage, we apply stratified sampling, ensuring that no single subject appears in both the training and testing datasets.

2.4. Feature Extraction

We consider two feature sets from the tracked keypoints: x- and y-coordinates of all keypoints and the angles between selected keypoints, based on Prakash et al. (2023) and further described in Appendix E.

Keypoint Coordinates The x- and y-coordinates of all labelled keypoints are treated independently as separate input channels, and used as a simple representation of the keypoint positions across frames.

Keypoint Angles The angles are calculated between pairs of keypoints to capture movement dynamics. We compute the dot product of vectors, normalizing by magnitudes, and applying a clipping function for valid angle calculations in radians.

2.5. Classification Models

This work explores three different classification models for GMA, using the extracted time series described in Section 2.4. 5-fold stratified cross-validation (CV) is performed across models to ensure robustness.

Table 1:	AUROC of various	classifiers for GM	I classification	across differen	t keypoint labellers.	The mean
	and standard deviat	ion over 30 seeds	is reported. B	Best result per r	nodel and labeller is	bolded.

Keypoint	Input Features	Early Infancy Group AUROC		Late Infancy Group AUROC			
Labeller		RF	LSTM	CNN	RF	LSTM	CNN
#1	Coord. Angles Both	0.6574 ± 0.19 0.8283 ± 0.13 0.7878 ± 0.14	0.6398 ± 0.16 0.6617 ± 0.16 0.6655 ± 0.16	0.7630 ± 0.19 0.8185 ± 0.14 0.7876 ± 0.17	0.3678 ± 0.25 0.5125 ± 0.25 0.3763 ± 0.24	0.4449 ± 0.23 0.6068 ± 0.21 0.4007 ± 0.19	0.5804 ± 0.23 0.3770 ± 0.22 0.5371 ± 0.22
#2	Coord. Angles Both	0.4907 ± 0.19 0.6763 ± 0.15 0.5737 ± 0.20	$egin{array}{l} 0.6807 \pm 0.17 \\ 0.6324 \pm 0.17 \\ 0.6088 \pm 0.16 \end{array}$	0.654 ± 0.19 0.6050 ± 0.19 0.6729 ± 0.20	0.4538 ± 0.24 0.6284 ± 0.20 0.4899 ± 0.23	0.4906 ± 0.24 0.4902 ± 0.22 0.5471 ± 0.18	0.5096 ± 0.20 0.6908 ± 0.22 0.5888 ± 0.20
#3	Coord. Angles Both	0.5874 ± 0.21 0.8105 ± 0.12 0.7278 ± 0.18	0.6176 ± 0.18 0.5621 ± 0.16 0.662 ± 0.21	0.7493 ± 0.20 0.8138 ± 0.14 0.7846 ± 0.17	0.5179 ± 0.27 0.6267 ± 0.22 0.5651 ± 0.18	0.4286 ± 0.27 0.5351 ± 0.23 0.4762 ± 0.25	0.6196 ± 0.19 0.5915 ± 0.24 0.5392 ± 0.29
Mean	Coord. Angles Both	0.5785 0.7717 0.6964	0.6460 0.6187 0.6454	0.7221 0.7458 0.7484	0.4465 0.5892 0.4771	0.4547 0.5440 0.4747	0.5699 0.5531 0.5550

1D Convolutional Neural Network (1D-CNN)

1D-CNNs are a variant of the more common 2D convolutional neural network, which apply convolution operations to 1D signals, making them well-suited for processing time-series data. These networks have been shown to perform well when working with smaller labelled datasets and for specific applications (Kiranyaz et al., 2021).

Long Short-Term Memory (LSTM) LSTM networks (Hochreiter and Schmidhuber, 1997) are a type of recurrent neural network capable of exploiting the temporal aspect of our data by learning relevant context information from previously seen time points. LSTMs are ideal for handling time series and assessing whether longer temporal memory helps in recognizing and classifying infant's general movements.

Random Forest (RF) RFs (Breiman, 2001) are powerful discriminative classifiers that perform well on a variety of datasets with minimal tuning (Biau and Scornet, 2016). It is an ensemble method that builds multiple decision trees trained on a random subset of data and combines their outputs to improve prediction accuracy and reduce overfitting. Although they do not explicitly account for the temporal structure of the data, their efficiency and accuracy make them a strong candidate for our classification tasks.

3. Experiments and Results

3.1. Implementation details

We performed a grid search over the hyperparameter space for each of the three classifier types in Section 2.5, choosing the values that performed best in the evaluation. The final models were trained using these hyperparameters with 5-fold stratified CV, and the results from the held-out test set, with 20% of the data, were collected. The classification models used included a 1D-CNN with binary cross entropy (BCE) loss, learning rate of 0.00001, batch size 6, a fullyconnected bottleneck with 150 features, and trained for 150 epochs. The LSTM used the BCE loss, learning rate 0.001, batch size 6, 3 layers, a hidden size of 64 and trained for 200 epochs. Finally, the random forest had 170 estimators. All experiments were run using 30 independent seeds on each individual set. Our models were implemented using pytorch v2.3.1 and scikit-learn v1.3.0. The final classification was evaluated using accuracy, Area Under the Receiver Operating Characteristic Curve (AUROC), and Area Under the Precision–Recall curve (AUPRC).

3.2. Results

Table 1 shows the results of the different classification models, for each labeller individually as well as averaged, measured in AUROC. See Appendix F for a comprehensive overview of AUPRC and accuracy in each task. They demonstrate a variety of outcomes

across age groups and feature sets, with no clear pattern indicating that one method is superior. However, the use of angle features, either isolated or combined, proves useful. Additionally, the early group shows significantly better overall results, showing a big difference in the difficulty of the task across age groups. One of the key takeaways from this study is that despite the relatively small and heterogeneous dataset, our approach has shown success in automatically classifying GM in newborns, with average AUROCs of up to 0.8283 in certain scenarios, opening promising lines of research for GMA "in the wild".

4. Conclusion and Future Outlook

In conclusion, our study demonstrates that we can successfully predict GMA with a promising AUROC of up to 0.8283, with performance generally better for the early group. This highlights the potential of using automated methods to assess infant motor behaviour. Despite the challenges posed by diverse data sources and recording conditions in the data. our results show that automated GMA is feasible in real-world clinical settings. This is a significant step forward in the early detection of neurodevelopmental disorders. This study lays the groundwork for further advancements, emphasizing the need for larger datasets and more refined models and feature extraction approaches to capture the data complexities. Ultimately, the goal is to enhance early prediction of neurodevelopmental diseases, offering a valuable tool for clinicians and ultimately improving patient care.

One of the key weaknesses of this study is the relatively small dataset, which limits the robustness and generalizability of our results, as indicated by relatively large standard deviations across folds. Moreover, the heterogeneity of the data makes the problem more challenging, while broadening its impact in the clinics. Expanding the dataset would allow us to explore more sophisticated methods, such as Multiple Instance Learning (MIL), which could introduce interpretability by making predictions on a per-episode basis. Additionally, using Vision Transformers to directly process the videos could better capture spatial and temporal patterns, further improving classification accuracy. Future work within the current dataset could focus on developing further features from the extracted keypoints and exploring other model classes to leverage the temporal structure in the task.

Acknowledgments

DC is funded from the Strategic Focal Area "Personalized Health and Related Technologies (PHRT)" grant #2021-911 of the ETH Domain (Swiss Federal Institutes of Technology), and SL and KC from the Swiss State Secretariat for Education, Research and Innovation (SERI), contract #MB22.00047. The authors would like to thank Ričards Marcinkevičs and Heike Leutheuser for their insights and discussions on the development of this manuscript.

References

Walter Baccinelli, Maria Bulgheroni, Valentina Simonetti, Francesca Fulceri, Angela Caruso, Letizia Gila, and Maria Luisa Scattoni. Movidea: A software package for automatic video analysis of movements in infants at risk for neurodevelopmental disorders. Brain sciences, 10(4):203, 2020.

Gérard Biau and Erwan Scornet. A random forest guided tour. *Test*, 25:197–227, 2016.

L Breiman. Random forests. Machine Learning, 2001.

Carl Doersch, Ankush Gupta, Larisa Markeeva, Adria Recasens, Lucas Smaira, Yusuf Aytar, Joao Carreira, Andrew Zisserman, and Yi Yang. Tapvid: A benchmark for tracking any point in a video. Advances in Neural Information Processing Systems, 35:13610–13626, 2022.

Christa Einspieler and Heinz FR Prechtl. Prechtl's assessment of general movements: a diagnostic tool for the functional assessment of the young nervous system. Mental retardation and developmental disabilities research reviews, 11(1):61–67, 2005.

Sepp Hochreiter and Jürgen Schmidhuber. Long short-term memory. *Neural computation*, 9(8): 1735–1780, 1997.

Muhammad Tausif Irshad, Muhammad Adeel Nisar, Philip Gouverneur, Marion Rapp, and Marcin Grzegorzek. Ai approaches towards prechtl's assessment of general movements: A systematic literature review. *Sensors*, 20(18):5321, 2020.

Serkan Kiranyaz, Onur Avci, Osama Abdeljaber, Turker Ince, Moncef Gabbouj, and Daniel J Inman. 1d convolutional neural networks and applications: A survey. *Mechanical systems and signal process*ing, 151:107398, 2021.

- Varun Ganjigunte Prakash, Manu Kohli, Aragulla Prasad Prathosh, Monica Juneja, Manushree Gupta, Smitha Sairam, Sadasivan Sitaraman, Anjali Sanjeev Bangalore, John Vijay Sagar Kommu, Lokesh Saini, et al. Video-based real-time assessment and diagnosis of autism spectrum disorder using deep neural networks. *Expert Systems*, page e13253, 2023.
- Kamini Raghuram, Silvia Orlandi, Paige Church, Maureen Luther, Alex Kiss, and Vibhuti Shah. Automated movement analysis to predict cerebral palsy in very preterm infants: an ambispective cohort study. *Children*, 9(6):843, 2022.
- Simon Reich, Dajie Zhang, Tomas Kulvicius, Sven Bölte, Karin Nielsen-Saines, Florian B Pokorny, Robert Peharz, Luise Poustka, Florentin Wörgötter, Christa Einspieler, et al. Novel ai driven approach to classify infant motor functions. Scientific Reports, 11(1):9888, 2021.
- William Thomas Schmidt, Matthew Regan, Michael C Fahey, and Andrew Paplinski. General movement assessment by machine learning: why is it so difficult? *Journal of Medical Artificial Intelligence*, 2(July):15, 2019.
- Nelson Silva, Dajie Zhang, Tomas Kulvicius, Alexander Gail, Carla Barreiros, Stefanie Lindstaedt, Marc Kraft, Sven Bölte, Luise Poustka, Karin Nielsen-Saines, et al. The future of general movement assessment: The role of computer vision and machine learning—a scoping review. Research in developmental disabilities, 110:103854, 2021.

Appendix A. Extended Dataset Description

In this section we present additional details about our dataset to the best of our ability. Some details are not available to us, such as weight at video for early group infants. Table 2 shows several demographic characteristics, as well as details about the videos themselves for both the early and late groups. Figure 3 provides histograms for the distributions of both video resolution and FPS for the early and late video groups.

Appendix B. Keypoint Labelling Tool

Figure 5 illustrates the keypoints used in this study and the labelling tool developed.

Appendix C. Keypoint Tracking

We adopt the work by Doersch et al. (2022) for keypoint tracking. Their model, TAP-Net, is designed to track arbitrary physical points on surfaces over video sequences. It is trained on a mix of synthetic and real-world datasets. The primary training datasets are synthetic, including TAP-Vid-Kubric, which contains simulated videos with physically realistic interactions between deformable and rigid objects, and TAP-Vid-RGB-Stacking, a robotic environment with teleoperated geometric shapes, focusing on challenges like tracking textureless and symmetric objects. These datasets provide perfect ground-truth point tracks, enabling TAP-Net to learn precise point tracking in complex, occlusion-prone scenarios. It uses a cost-volume-based architecture, inspired by optical flow methods, to track point motion across frames by comparing dense feature grids at query points. The network is trained with two objectives: (1) Point location regression, using Huber loss to estimate the query point's position and ensure precise tracking, and (2) Occlusion classification, using cross-entropy loss to predict when the point is occluded, enabling the model to handle occlusion scenarios effectively. TAP-Net is validated and tested on real-world datasets like TAP-Vid-Kinetics, which includes diverse human actions and complex scenes, and TAP-Vid-DAVIS, which focuses on challenging segment and object tracking tasks.

Appendix D. Outlier Detection

To mitigate potential errors from the tracking tool, we implemented a tool that automatically flags any sudden, unrealistic movements of keypoints. Specifically, we define such movements as coordinate changes that exceed 15 times the overall standard deviation for each keypoint. This threshold is set deliberately high to avoid flagging normal, natural movements, as well as fidgety movements that can inherently exhibit high magnitudes without indicating error.

Once flagged, the affected keypoints are relabeled and subsequently retracked. This process is iteratively applied up to three times, as we observed only marginal improvements in performance after three rounds in the final detection task.

In general, this outlier-detection process can be structured to run for a set number of iterations, until a defined performance tolerance is reached, or until no further outliers are identified, ensuring the accuracy of the tracked coordinates.

Appendix E. Feature Extraction

In this work, we perform the classification task on a set of features extracted from the obtained keypoints. In particular, we study the classification on three subsets, as reported in our results:

- Coord. The keypoint coordinates, that correspond to the x- and y-locations of all keypoints, as listed in Figure 4.
- Angles The angles between keypoints of interest. The values of the angle corresponding to each keypoint pair are provided separately to the model.

Given keypoints \mathbf{p}_1 , \mathbf{p}_2 , and \mathbf{p}_3 with coordinates (x_1, y_1) , (x_2, y_2) and (x_3, y_3) respectively. We would like to compute the angle between \mathbf{p}_1 and \mathbf{p}_3 at middle point \mathbf{p}_2 . Thus, we define

$$\mathbf{v}_1 = \begin{bmatrix} x_1 - x_2 \\ y_1 - y_2 \end{bmatrix}, \quad \mathbf{v}_2 = \begin{bmatrix} x_3 - x_2 \\ y_3 - y_2 \end{bmatrix}.$$

Then, the angle θ between the two vectors can be computed as:

$$\theta = \arccos\left(\frac{\mathbf{v}_1 \cdot \mathbf{v}_2}{\|\mathbf{v}_1\| \|\mathbf{v}_2\|}\right),$$

Table 2: Calculated demographic and video characteristics

Characteristic	Early Group	Late Group
Age at video recording (Days) (mean, stddev)	30.9, 19.9	170.4, 24.8
Post-menstrual age at video recording (Days) (mean, stddev)	231.5, 6.5	N/A
Corrected Age at video recording (Days) (mean, stddev)	N/A	92.5, 17.4
Weight at video recording (g) (mean, stddev)	N/A	4148.2, 830.7
Video Length (s) (mean, stddev)	409, 144	224, 93
FPS (min, max)	30, 120	30, 120
Extremely Preterm	16	15
Very Preterm	20	19
Moderate to Late Preterm	3	3
Not Preterm	0	0

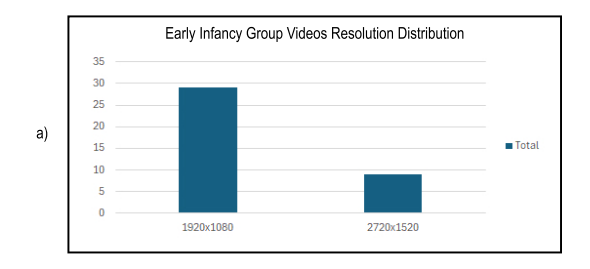
where $\mathbf{v}_1 \cdot \mathbf{v}_2$ is the dot product of the vectors and $\|\mathbf{v}_1\|$ and $\|\mathbf{v}_2\|$ are the magnitudes (or norms) of the vectors.

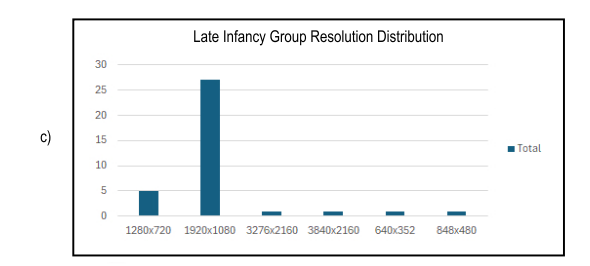
Table 3 provides the list of the studied angle sets, which keypoints they are formed by, and a brief intuitive explanation. The angles are illustrated in 6.

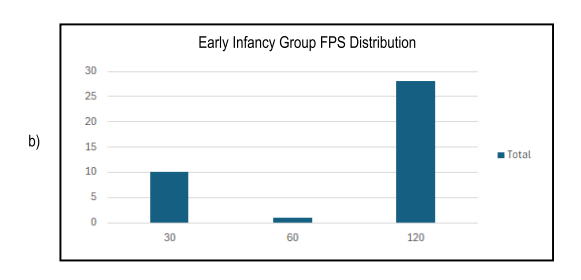
• **Both** The combination of both coordinates and angles, shown as "both" in the results.

Appendix F. Further results

Table 4 and Table 5 show the results of the presented classification models, for each labeller individually as well as averaged, grouped by age and feature extraction method used, measured in AUPRC and accuracy, respectively. The best performing method per task is marked in bold and overall both metrics resemble the behaviour of the AUROCs reported in the main text in Table 1.







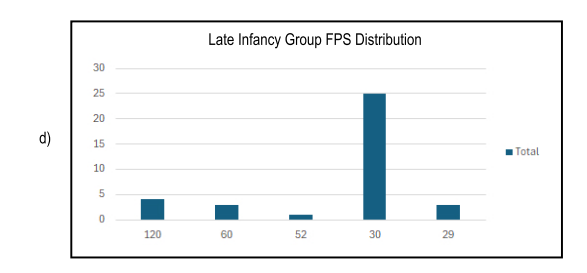


Figure 3: Histograms showing the distributions of a) early infancy group video resolution, b) early infancy group video FPS, c) late infancy group video resolution, and d) late infancy group video FPS

Figure 4: List of all and extreme keypoints considered in this study, coloured by label on the right.

label off the right.						
All Keypoints	Extreme					
nose						
head bottom						
head top	x					
left ear						
right ear						
left shoulder						
right shoulder						
left elbow	x					
right elbow	x					
left wrist	x					
right wrist	x					
left hip						
right hip						
left knee	\mathbf{x}					
right knee	x					
left ankle	x					
right ankle	x					



Figure 5: Example of frame with labelled keypoints.

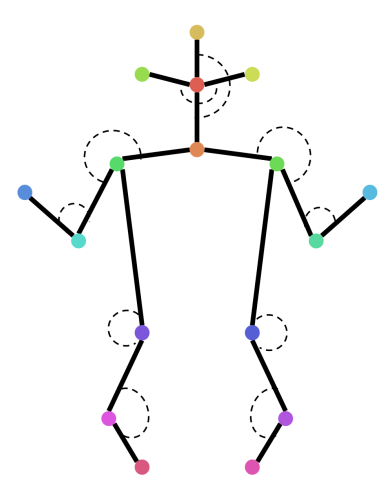


Figure 6: Illustration of the angle features. The dash lines show the angles that we compute in the set of angle features.

\mathbf{p}_1	\mathbf{p}_2	\mathbf{p}_3	Explanation
head top	nose	head bottom	Head top to neck angle
right ear	nose	left ear	Right to left ear angle
left elbow	left shoulder	head bottom	Head to left shoulder angle
right elbow	right shoulder	head bottom	Head to right shoulder angle
left wrist	left elbow	left shoulder	Left elbow angle
right wrist	right elbow	right shoulder	Right elbow angle
left knee	left hip	left shoulder	Left hip angle
right knee	right hip	right shoulder	Right hip angle
left hip	left knee	left ankle	Left knee angle
right hip	right knee	right ankle	Right knee angle

Table 3: List of angle components used in the study with intuitive explanations.

Table 4: Results. AUPRC over 30 seeds is reported. The best result for each model and labeller is bolded.

		Early Infancy Group			Late Infancy Group			
Labeller	Features	AUPRC			AUPRC			
		RF	LSTM	CNN	RF	LSTM	CNN	
	Coord.	0.7733 ± 0.14	$\boldsymbol{0.7503 \pm 0.13}$	0.8585 ± 0.11	0.2589 ± 0.14	0.3603 ± 0.22	$\textbf{0.4627} \pm \textbf{0.23}$	
1	Angles	$\boldsymbol{0.8856 \pm 0.09}$	0.7346 ± 0.16	$\boldsymbol{0.8772 \pm 0.1}$	$\boldsymbol{0.389 \pm 0.25}$	$\boldsymbol{0.47 \pm 0.24}$	0.266 ± 0.17	
	Both	0.8575 ± 0.09	0.7359 ± 0.15	0.8547 ± 0.13	0.2879 ± 0.19	0.2938 ± 0.15	0.3983 ± 0.22	
	Coord.	0.665 ± 0.14	$\boldsymbol{0.7798 \pm 0.14}$	$\boldsymbol{0.799 \pm 0.12}$	0.3142 ± 0.18	0.38 ± 0.27	0.4778 ± 0.24	
2	Angles	$\boldsymbol{0.7703 \pm 0.13}$	0.7097 ± 0.17	0.6867 ± 0.16	$\boldsymbol{0.4674 \pm 0.25}$	$\boldsymbol{0.3814 \pm 0.22}$	0.4959 ± 0.27	
	Both	0.7088 ± 0.15	0.7105 ± 0.15	0.7955 ± 0.14	0.3523 ± 0.18	0.3804 ± 0.22	0.4638 ± 0.25	
	Coord.	0.7259 ± 0.15	0.6986 ± 0.17	0.8522 ± 0.13	0.3593 ± 0.19	0.3405 ± 0.23	$\boldsymbol{0.5538 \pm 0.21}$	
3	Angles	$\boldsymbol{0.8685 \pm 0.09}$	0.6655 ± 0.16	0.85 ± 0.14	$\boldsymbol{0.4929 \pm 0.28}$	$\boldsymbol{0.4194 \pm 0.24}$	0.4061 ± 0.25	
	Both	0.8121 ± 0.13	$\boldsymbol{0.7461 \pm 0.17}$	$\boldsymbol{0.8579 \pm 0.12}$	0.3603 ± 0.18	0.3838 ± 0.22	0.4269 ± 0.27	
	Coord.	0.7214	0.7429	0.8366	0.3108	0.3603	0.4981	
Mean	Angles	0.8415	0.7033	0.8046	0.4498	0.4236	0.3893	
	Both	0.7928	0.7308	0.8360	0.3335	0.3527	0.4297	

Table 5: Results. Accuracy over 30 seeds is reported. The best result for each model and labeller is bolded.

		Early Infancy Group			Late Infancy Group			
Labeller	Features	Accuracy			Accuracy			
		RF	LSTM	CNN	RF	LSTM	CNN	
	Coord.	0.5962 ± 0.16	0.59 ± 0.15	0.6946 ± 0.15	0.5759 ± 0.14	0.5793 ± 0.11	0.6133 ± 0.16	
1	Angles	$\boldsymbol{0.7266 \pm 0.13}$	0.5978 ± 0.14	$\boldsymbol{0.7047 \pm 0.16}$	$\boldsymbol{0.6305 \pm 0.17}$	$\boldsymbol{0.6785 \pm 0.13}$	0.5701 ± 0.13	
	Both	0.6596 ± 0.15	$\boldsymbol{0.6444 \pm 0.16}$	0.6849 ± 0.12	0.6073 ± 0.16	0.5809 ± 0.16	$\boldsymbol{0.6168 \pm 0.15}$	
	Coord.	0.4542 ± 0.17	0.5973 ± 0.15	0.6219 ± 0.13	0.6385 ± 0.13	0.5856 ± 0.15	0.5603 ± 0.21	
2	Angles	$\boldsymbol{0.6518 \pm 0.14}$	0.5594 ± 0.14	0.5568 ± 0.17	$\boldsymbol{0.6765 \pm 0.08}$	0.6297 ± 0.14	$\boldsymbol{0.6432 \pm 0.13}$	
	Both	0.5268 ± 0.18	0.5871 ± 0.16	$\boldsymbol{0.6275 \pm 0.15}$	0.6444 ± 0.13	$\boldsymbol{0.6418 \pm 0.14}$	0.6113 ± 0.16	
	Coord.	0.5548 ± 0.18	0.6125 ± 0.14	0.6764 ± 0.14	0.6652 ± 0.14	0.5955 ± 0.15	0.614 ± 0.19	
3	Angles	$\boldsymbol{0.6995 \pm 0.11}$	0.5443 ± 0.15	$\boldsymbol{0.7508 \pm 0.12}$	$\boldsymbol{0.6995 \pm 0.08}$	0.6233 ± 0.16	0.638 ± 0.12	
	Both	0.6186 ± 0.17	$\boldsymbol{0.6502 \pm 0.17}$	0.7101 ± 0.14	0.6605 ± 0.09	$\boldsymbol{0.6505 \pm 0.17}$	$\boldsymbol{0.6393 \pm 0.13}$	
Mean	Coord.	0.5351	0.5999	0.6643	0.6265	0.5868	0.5959	
	Angles	0.6926	0.5672	0.6708	0.6688	0.6438	0.6171	
	Both	0.6017	0.6272	0.6742	0.6374	0.6244	0.6225	